A comparison of CsI:Tl and GOS in a scintillator-CCD detector for nuclear medicine imaging

A comparison of CsI:Tl and GOS in a scintillator-CCD detector for nuclear medicine imaging

S.L. Bugby,[a,1] **L. K. Jambi**[a,b] **and J.E. Lees**[a]

[a]*Department of Physics & Astronomy, University of Leicester,*
Leicester, LE1 7RH, U.K.

[b]*Department of Radiological Sciences, College of Applied Medical Sciences, King Saud University,*
Riyadh, Kingdom of Saudi Arabia

E-mail: s.bugby@le.ac.uk

ABSTRACT: A number of portable gamma cameras for medical imaging use scintillator-CCD based detectors. This paper compares the performance of a scintillator-CCD based portable gamma camera with either a columnar CsI:Tl or a pixelated GOS scintillator installed.

The CsI:Tl scintillator has a sensitivity of 40% at 140.5 keV compared to 54% with the GOS scintillator. The intrinsic spatial resolution of the pixelated GOS detector was 1.09 mm, over 4 times poorer than for CsI:Tl. Count rate capability was also found to be significantly lower when the GOS scintillator was used. The uniformity was comparable for both scintillators.

KEYWORDS: Gamma camera, SPECT, PET PET/CT, coronary CT angiography (CTA); Gamma detectors (scintillators, CZT, HPG, HgI etc); Scintillators and scintillating fibres and light guides; Scintillators, scintillation and light emission processes (solid, gas and liquid scintillators)

---

[1]Corresponding author.

Contents

1 Introduction

In nuclear medical imaging, advances in detector technology have led to the development of a range of small field of view (SFOV) gamma cameras. These cameras are designed for intraoperative use (such as for sentinel lymph node biopsy) or as dedicated small-organ systems (such as for thyroid and parathyroid imaging) [1]. All cameras are designed to have the highest possible sensitivity — for detection of low activity features — and the best spatial resolution — to differentiate and localise regions of interest. The improvement of sensitivity and spatial resolution is often mutually exclusive, and a large amount of interest in both detector and collimator design is focussed on improving the trade-off between the two. There is also a drive towards reducing the size and weight of the typical components in a gamma camera to allow use within the restricted space of the operating theatre [1].

A traditional large field of view (LFOV) medical gamma camera uses a NaI:Tl scintillator-based detector, coupled to an array of photomultiplier tubes (PMTs) [2]. Many SFOV cameras use direct semiconductor detection — typically using materials such as CdTe or CZT which have high

detection efficiencies for the photon energies found in nuclear medicine [3–6]. A number of SFOV cameras are scintillator-based, and may use position sensitive PMTs [7–10], photodiodes [11, 12], Si-PMs [13], or charge coupled devices (CCDs) [14, 15]. As SFOV detectors are much smaller than their LFOV counterparts, they are able to use scintillators such as CsI:Tl or CsI:Na — which are of particular interest as they can be grown in columnar structures, reducing light spreading and so improving spatial resolution [16] — or newer ceramic scintillators (such as GOS) with good absorption properties. For scintillators which can't be grown in a columnar structure, powdered or single crystals can be arranged to form a pixelated detector to decrease light spread. As the cross-sectional areas of grown columnar structures are smaller than manufactured pixels, they show more of a reduction in light spread; pixelated detectors however may use reflective coatings to eliminate cross-talk between channels.

In this paper, we present a characterisation of a SFOV gamma camera with a pixelated GOS scintillator and compare this to results obtained with a columnar CsI:Tl scintillator fitted in the same CCD detector.

2 Materials and Methods

2.1 Camera

The Compact Gamma Camera (CGC) has been designed at the University of Leicester, in collaboration with the University of Nottingham, as a portable medical imaging gamma camera. The CGC uses a scintillator-based detector and has previously been fully characterised with a 600 μm thick CsI:Tl scintillator [17] using a set of protocols designed for the investigation of SFOV gamma camera performance [18]. These protocols form the basis of the experimental methods used in this investigation.

In the CGC, the scintillator is coupled to an e2v CCD97 electron multiplying CCD (EMCCD) back-thinned to improve sensitivity [19]. The incorporation of an on-chip gain stage in the EMCCD reduces the effects of read noise. The EMCCD pixels (16 μm × 16 μm) have been binned (×4) to produce 64 μm × 64 μm square pixels, in a 128 × 128 array. The back of the CCD is thermally coupled to a thermoelectric cooler (TEC), which is itself coupled to a phase-change material. This maintains the CCD at < −10°C for extended periods of operation, improving noise statistics.

The CGC detector is placed within an Al chamber which is held at a typical pressure of the order of 1 Pa. This allows for the continued use of hygroscopic scintillators, such as CsI:Tl, with limited deterioration, and improves the cooling performance of the system. The chamber is surrounded by 3 mm thick tungsten shielding.

A 6 mm thick tungsten collimator, with a 1 mm diameter, 60° acceptance angle, knife edge pinhole is used for imaging to increase the detector FOV. In many extrinsic measurements, results are dominated by the performance of the collimator rather than the detector however these are included in the presented results since these are the characteristics most interesting to a medical practitioner.

2.1.1 Scintillators

A 1500 μm thick Hammatsu CsI:Tl scintillator [20] was used for this study. This scintillator has been produced with a columnar structure, with tightly packed narrow needles of CsI:Tl crystal.
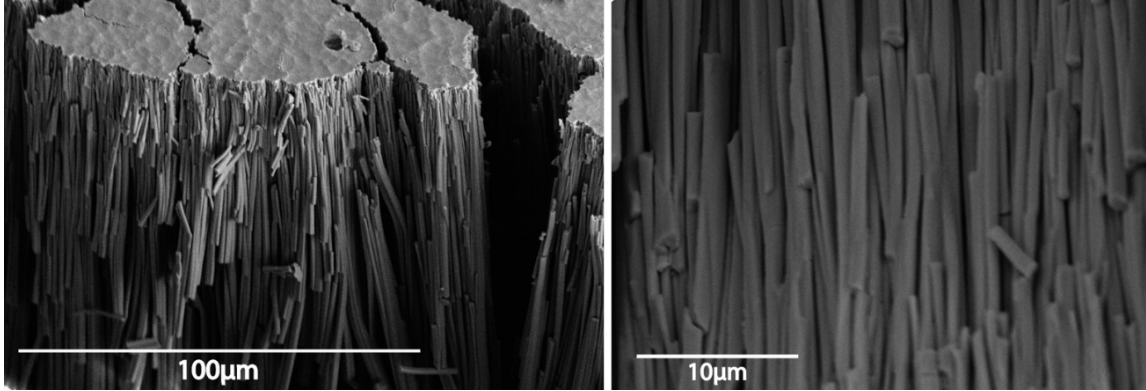
Figure 1. Scanning electron microscope images of cleaved edge of CsI:Tl scintillator. Tightly packed columns with approximately 1 μm diameter extend vertically through the thickness of the scintillator.

Figure 1 shows scanning electron microscope images of a section of the scintillator, showing these features. The columns are intended to act as light guides with total internal reflection acting to channel optical photons towards the CCD and reduce light spread within the scintillator.

The CsI:Tl is backed onto a 500 μm thick amorphous carbon substrate. The substrate is mirrored to increase light collection, redirecting light back towards the CCD.

The GOS (Gd$_2$O$_2$S:Pr) scintillator was manufactured to our required dimensions by Toshiba [21]. The total scintillator package size is 8 mm × 8 mm × 1500 μm. Within the scintillator package is an array of 18 × 18 GOS pixels, each 400 μm square, separated by 40 μm thick reflectors painted with TiO$_2$ to constrain scintillation photons within each pixel. A section of this array is shown in figure 2.

There are a number of factors that determine the suitability of a scintillator for a particular application. The greater the density and attenuation coefficient of the material, the greater the absorption of incident photons. Light yield indicates the number of scintillation photons that would be expected from a given energy input (affected strongly by scintillator composition) — the more scintillation photons produced, the easier a single X- or gamma ray event is to detect and the better the theoretical limit for energy resolution. Peak emission wavelength and refractive index affect the efficiency with which a given detector can detect scintillation photons. These factors are compared for CsI:Tl and GOS in table 1 for 140.5 keV — the photopeak for ^{99m}Tc, the most common isotope used in nuclear medicine.

2.1.2 Coupling method

The scintillator is placed on the detecting area of the CCD and held in place with a flexible Kapton window. The method of scintillator-detector coupling used is known to have a significant effect on detector performance [26]. To ensure consistent testing conditions for the different scintillators with the same CCD, no optical grease or other coupling material was used.

2.2 Imaging process

A full image can consist of numerous frames, each taking ∼ 0.1 s to acquire. Images are stored in a proprietary event record format, which separates each image frame to allow for image processing.

Table 1. Comparison of some key properties of CsI:Tl and GOS scintillators. Theoretical sensitivity has been calculated using the Beer-Lambert Law and the densities and attenuation coefficients included in the table. NaI has been included as this is used in the vast majority of LFOV systems.

Parameter	NaI	CsI:Tl	GOS
Density (gcm^{-3})	3.67 [22]	4.51 [20]	7.3 [21]
Attenuation coefficient at 141 keV (cm^2g^{-1})	0.707 [23]	0.847 [23]	1.092 [23]
Photon yield (per keV)	38 [22]	52–66 [24]	35–50 [25]
Poisson limited energy resolution at 141 keV	3.2%	2.4–2.7%	2.8–3.3%
Peak emission wavelength (nm)	415 [22]	550 [20]	512 [21]
Refractive index at peak emission	1.85 [22]	1.79 [20]	2.2 [21]
Theoretical sensitivity to 141 keV photons (1500 μm thickness)	32.2%	43.6%	69.8%
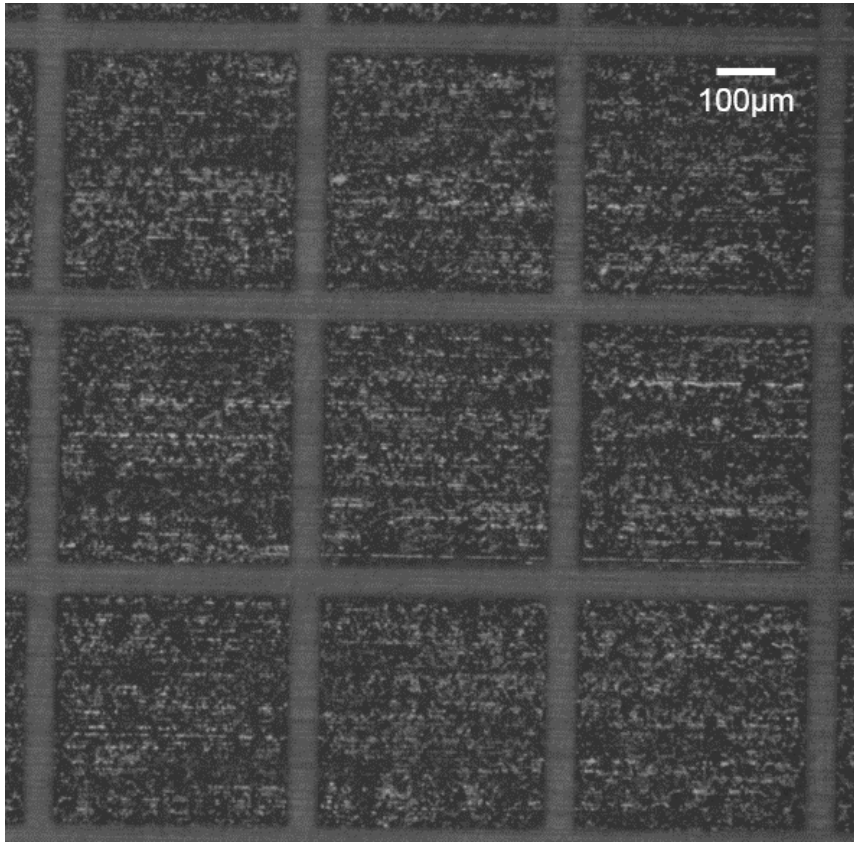
Figure 2. A 3×3 section of the pixelated GOS scintillator. Each pixel is 400 μm $\times$ 400 μm, with individual pixels separated by a 40 μm wide boundary material coated with TiO_2. The striations visible in the GOS pixels are due to the manufacturing process.

The image format records the x-position, y-position and signal level for each pixel in the frame which exceeds a pre-set threshold value.

Hot pixels were defined as those pixels recording counts above the expected thermal noise in more than 5% of frames in a dark image. Designated hot pixels are removed from each frame during the acquisition process.

After acquisition, images can be processed to convert the pixel signals on the CCD to an image that displays the magnitude and position of deposited energy throughout the acquisition time. The post-processing used depends on the type of scintillator installed.

2.2.1 Gamma reconstruction for CsI:Tl

When columnar CsI:Tl is installed in the CGC, each gamma photon interaction within the scintillator produces an approximately Gaussian light splash on the CCD [27], with a typical width between two and ten pixels (see figure 3a). The signal within each light splash is higher than the detector noise and so thermal and readout noise can be excluded during acquisition by setting a threshold equal to the mean of the noise peak plus 5σ.

The intensity of each light splash (and so the energy of each incident gamma photon) is calculated using an automatic scale selection algorithm often referred to as blob detection [27]. This algorithm identifies each light splash and calculates a representative Gaussian distribution with a peak amplitude A and standard deviation σ. The energy of the incident gamma photon is derived from the total signal within each light splash — given by $2\pi A\sigma^2$ — and a single gamma event is placed at the centroid of the light splash [27].
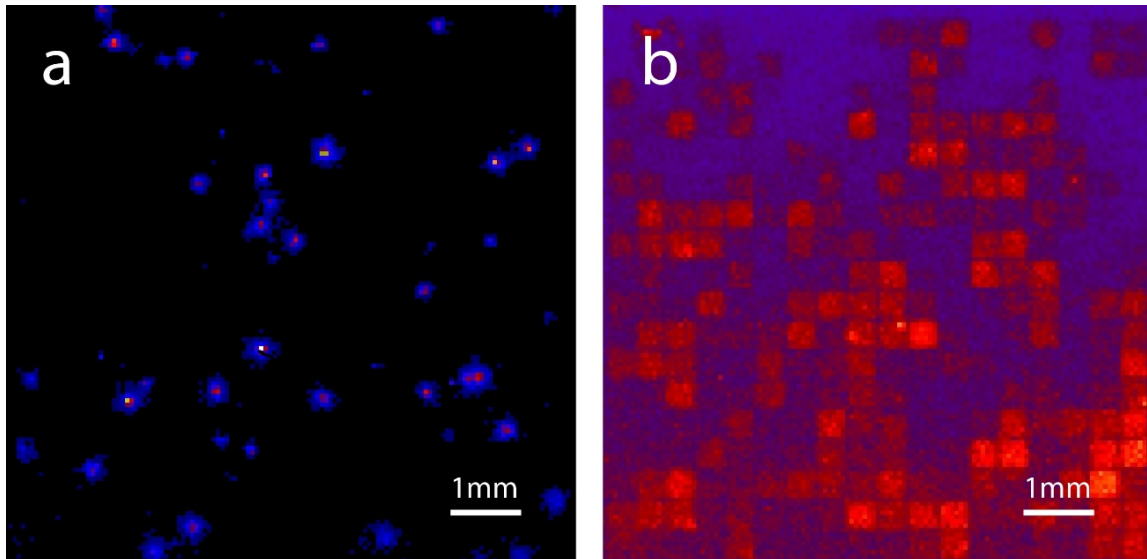
Figure 3. Single frame images of a ^{99m}Tc flood source taken with a) CsI:Tl and b) GOS scintillators installed. The spread of scintillation light in the CsI:Tl is limited by its columnar structure whereas the GOS scintillation photons are constrained within the manufactured pixels. Note that in both cases a large number of scintillation photons have been detected but reconstruction is needed to equate these to individual gamma interactions.

2.2.2 Gamma reconstruction for GOS

With the GOS pixelated scintillator installed in the CGC, each gamma photon interaction within the scintillator produces a number of scintillator photons which are constrained within the GOS pixel in which the interaction occurs (see figure 3b). The $400\,\mu$m square GOS pixels each cover approximately 49 CCD pixels. The lower scintillation photon yield of GOS compared to CsI:Tl,

along with the larger area over which the light is typically spread, means that signal levels within each CCD pixel are not significantly higher than the background noise and so thresholding is not applied during acquisition.

After installation of the GOS scintillator, the area of the CCD corresponding to each GOS pixel was determined. During gamma reconstruction, the CCD image was binned into an 18×18 pixel image corresponding to the GOS array. In contrast with the CsI:Tl acquisition, where only events above a threshold are recorded, this method records a signal in each pixel in every frame however many of these will not be due to a gamma event.

2.2.3 Further image correction

After gamma reconstruction, an energy window is typically applied to exclude noise and scattered photons. Due to the energy resolution of the system of $> 54\%$ at the energy investigated [17], this could not be applied to data from the CGC. Instead, image reconstruction was carried out on a background image taken over ~ 30 minutes. The resulting spectrum of this image was fitted with a Gaussian curve to identify the noise peak. During image analysis, only events with an energy greater than the mean of the noise peak plus 5σ were used. In practice, this excluded very few events from the CsI:Tl images (as detector noise had already been thresholded during acquisition). This technique means that the scattered and fluorescence photons that would ideally be excluded from the image are included in this analysis — the energy resolution of the system and implications of this are discussed in section 4.

Dark images, with no incident illumination, were taken regularly during experimentation, and an appropriate dark image (corrected for any difference in exposure time) was subtracted before further analysis. A master flat image was then created by subtracting an appropriate dark image from a flood image and normalizing the resulting image to its maximum value. Images could then be corrected for flat field effects by dividing by this master flat image.

A portion of the image containing a known defect on the CCD was excluded from analysis.

2.3 Experimental setup

The characterisation parameters investigated were spatial resolution (intrinsic and extrinsic), sensitivity (intrinsic and extrinsic), count rate capability and intrinsic signal uniformity. The images acquired to achieve this are described below — the rationale behind the setup used has been described in more detail previously [17, 18].

Characterisation was performed using ^{99m}Tc — a common isotope in medical imaging with a photopeak energy of 140.5 keV and a half-life of six hours. A ^{99m}Tc-pertechnate solution was provided by the Nuclear Medicine Department, Leicester Royal Infirmary, with varying concentrations. The solution was used to fill a 2 mm diameter, 5 mm depth, well source and the contained activity was measured with a CAPINTEC CRC-55tR dose calibrator. The activity used for each characterisation test is given in table 2. In each case the starting activity has been given — for long and multiple acquisitions this starting activity decayed during the course of the experiment and calculations took this into account. Count rate capability was measured first with a source activity that could be seen to saturate the detector, for further tests activities were used within the count rate capability of the detector.

Table 2. Activity used for characterisation tests.

Parameter	Activity used (MBq)	
	CsI:Tl	GOS with direct coupling
Intrinsic sensitivity and intrinsic uniformity	1.35	14.0
Count rate capability	72.0	72.6
Intrinsic spatial resolution	1.35	14.0
Extrinsic sensitivity and extrinsic spatial resolution	1.35	1.7

2.3.1   Count rate capability

The point source was placed at a distance of 100 mm from the detector. The activity contained within the point source was chosen to ensure that the image was initially saturated. A 2000 frame (approximately 3 1/2 minute) image was acquired every hour for several days until the source had decayed to an undetectable level.

Counts per second incident on the detector were calculated using solid angle formulae and plotted against recorded counts per second. The maximum recorded count rate and the point at which the count rate capability curve deviated from a straight line by more than 20% were calculated. As the full image was not used for this analysis due to a CCD defect (section 2.2.3), the recorded rates were calculated per pixel and then multiplied by the total number of pixels on the CCD.

2.3.2   Intrinsic sensitivity and intrinsic uniformity

The point source was placed at a distance of 100 mm from the detector and imaged over 20000 frames (approximately 34 minutes).

Solid angle formulae were used to determine the incident counts on the detector allowing intrinsic sensitivity to be reported as a percentage of incident counts as previously described [17].

2.3.3   Intrinsic spatial resolution

A 10 mm thick lead transmission mask, containing a 3 mm × 20 mm rectangular slit was placed on the camera face — at a distance of 7 mm from the detector. The point source was placed at a distance of 200 mm from the detector. Although the mask was placed as close to the detector as possible some spreading of photons between the mask and the detector are expected. The geometry of the setup used would be expected to artificially degrade the measured intrinsic spatial resolution by ∼ 75 μm for a centred source. Images were recorded over 5000 frames (8 1/2 minutes).

The resulting slit images were analysed using the edge response function technique to produce a line spread function (LSF) [17]. The full width half maximum (FWHM) and full width tenth maximum (FWTM) of the resulting LSF were calculated. For more detail of this process and example images please see Bugby et al. 2014 [17].

2.3.4   Extrinsic spatial resolution

Extrinsic measurements were taken with a 1 mm diameter knife-edge pinhole collimator, with a 60° acceptance angle, placed at a distance of 10 mm from the detector. The point source was imaged over 2000 frame (approximately 3 1/2 minute) at 10 different distances from 20 mm to 200 mm

from the collimator face. Where possible, images were recorded both with and without Perspex filling the space between collimator and source, to a maximum thickness of 77.5 mm of Perspex.

Figure 4 shows examples of the point source images obtained with each detector. The resulting images of the point source were fitted with a 2-dimensional Gaussian. Spatial resolution was then defined as the mean FWHM of the fitted distribution. Spatial resolution was calculated using this technique for each measured distance, and these values were used to calculate the linear relationship between spatial resolution and imaging distance.
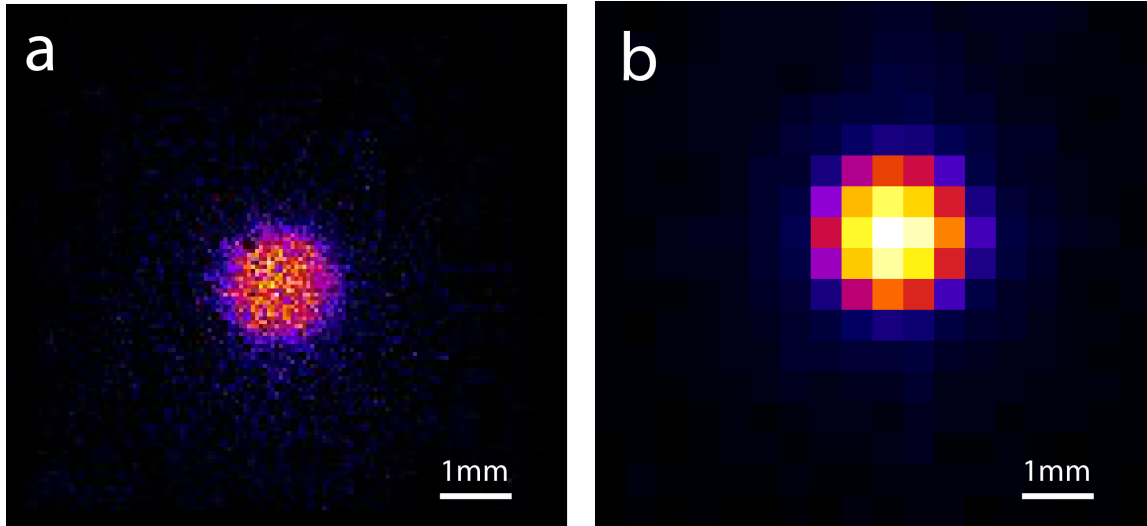
Figure 4. Example extrinsic point source images obtained using the CsI:Tl (a) and GOS (b) scintillator. The point source was imaged through 20 mm of Perspex. The given scale is of the detector image and hasn't been adjusted for the magnification of the pinhole collimator.

2.3.5 Extrinsic sensitivity

Extrinsic sensitivity was calculated with the same images as described for extrinsic spatial resolution.

During analysis for spatial resolution, a two dimensional Gaussian function was fitted to the image of the point source. This fit provided a background offset — attributed to scattered or fluorescence photons — which was subtracted from all pixels before sensitivity analysis. The counts recorded within the image were divided by the activity of the source to give sensitivity in cps/MBq. The reported parameter was sensitivity at a nominal distance of 50 mm from the collimator, both with and without scattering media.

3 Results

The performance characteristics for each scintillator are summarised in table 3. The most significant difference seen between the two types of scintillator was for intrinsic spatial resolution, which was calculated to be 230 μm for the CsI:Tl scintillator and 1090 μm for the GOS scintillator.

When looking at extrinsic resolution, a straight line provided a better fit to the CsI:Tl data (with a mean $R^2 > 0.999$) compared to GOS data ($R^2 > 0.995$) and the CsI:Tl results also provided a closer match to the theoretical geometric resolution of the 1 mm diameter pinhole collimator —

0.1d+1 [28]. This is due to the effect of the smaller intrinsic resolution for CsI:Tl. The fits tabulated in table 3 are for $d \leq 50$ mm to allow comparison at these distances and will not be representative at larger distances.

There is also a large difference in intrinsic sensitivity measurements, the CsI:Tl scintillator was found to have a sensitivity of 40% whereas the sensitivity for GOS was 54%. Both of these values are less than the theoretical maximum sensitivity (table 1).

Extrinsic sensitivity was also higher for the GOS scintillator although this showed a slightly larger reduction in counts when scattering material was introduced. The theoretical drop in detected counts through 50 mm of Perspex is ~ 57% [29]. Although this value is within the errors for both scintillators, the directly calculated drop for GOS was extremely close — 56% — whereas it was only 50% of CsI:Tl. This might suggest that a higher number of low energy events (e.g. fluorescence photons) are included in the CsI:Tl images.

Table 3. Performance characteristics for CGC with either a 1500 μm thick GOS or 1500 μm thick CsI:Tl scintillator installed.

Parameter		CsI:Tl	GOS
Intrinsic spatial resolution	FWHM	230 ± 25 μm	1090 ± 200 μm
Intrinsic sensitivity	At 140.5 keV	40 ± 3 %	54 ± 4 %
Intrinsic uniformity	Coefficient of variation	20 ± 15 %	17 ± 9 %
Extrinsic spatial resolution	At d mm from the collimator (no scattering material)	(0.0971 ± 0.0007)d + (0.83 ± 0.02)	(0.087 ± 0.004)d + (1.1 ± 0.3)
	At d mm from collimator (including scattering material)	(0.0946 ± 0.002)d + (1.07 ± 0.07)	(0.093 ± 0.006)d + (1.2 ± 0.4)
Extrinsic sensitivity	At 50 mm from collimator (no scattering material)	6.6 ± 0.5 cps/MBq	18.5 ± 0.3 cps/MBq
	At 50 mm from the collimator (including scattering material)	3.3 ± 0.5 cps/MBq	8.1 ± 0.3 cps/MBq
Count rate capability	Maximum recorded count rate	35700 ± 200 cps	3170 ± 30 cps
	Incident counts for 20% deviation from linear relationship	7210 ± 100 cps	3620 ± 200 cps

4 Discussion

There is often a trade off in the design of gamma detectors for medical imaging and the characterisation performed here shows that this is also the case with the scintillators tested.

From the characterisation performed in this paper, GOS would appear to be the better choice for clinical imaging when sensitivity is key however the pixel size does limit its utility for imaging. The CsI:Tl scintillator is a better choice when precise localisation of sources is required due to its superior intrinsic spatial resolution.

The utility of the GOS scintillator is also greatly limited by the count rate capability. The maximum number of individual events is constrained by the large size of the GOS pixels and the frame rate of the imaging electronics. Both spatial resolution and count rate capability of the

GOS pixelated scintillator could be improved by reducing the size of the GOS pixels, which is not currently a cost-effective solution.

An energy resolution of 54% at 140.5 keV has previously been reported for the CGC using a 600 μm thick CsI:Tl scintillator [17], whereas in the work described here the energy peak could not be resolved at all. This reduction in energy resolution compared to previously reported results requires further investigation. In previous tests, the scintillator was coupled to the CCD with a thin layer of optical grease and it may be that the improved coupling efficiency when this is used explains the improved energy resolution. The difference in performance with and without optical grease will be reported in a future paper.

The detector signal to noise contributes to the energy resolution that may be achieved with scintillators. A reduction in temperature of the detector would therefore also be expected to improve energy resolution. The operating temperature of the CGC is limited by the self-contained phase-change cooling system, chosen for portability and appropriateness for use in surgical theatre. At the temperatures the CGC can reach ($-10°$C minimum), signal levels, in particular for GOS, are close to the thermal noise background. Energy thresholding as used in this report (in contrast with the energy windowing more commonly used) can produce clinical images [30].

5   Conclusion

The performance of GOS and CsI:Tl scintillators in a portable medical imaging gamma camera has been evaluated and compared. The pixelated GOS scintillator was significantly more sensitive than the CsI:Tl but with a poorer spatial resolution and count rate capability. GOS would be most appropriate for use in low-signal situations where high sensitivity is required but spatial resolution is not of particular concern. The CsI:Tl scintillator is the better choice for situations where high spatial resolution is a necessity, particularly if there are few time constraints on the length of images to be recorded.

Further work is needed to determine whether better coupling between the scintillator and the CCD would improve the energy resolution and so improve the overall performance of the of the CGC.

References

[1] M. Tsuchimochi and K. Hayama, *Intraoperative gamma cameras for radioguided surgery: Technical characteristics, performance parameters, and clinical applications*, *Phys. Med.* **29** (2013) 126.

[2] R.S. Lawson, *The Gamma Camera: A comprehensive guide*, Institute of Physics and Engineering in Medicine, York, U.K. (2013).

[3] F. Sanchez et al., *Design and tests of a portable mini gamma camera*, *Med. Phys.* **31** (2004) 1384.

[4] P. Russo et al., *Evaluation of a CdTe semiconductor based compact gamma camera for sentinel lymph node imaging*, *Med. Phys.* **38** (2011) 1547.

[5] M. Tsuchimochi et al., *A prototype small CdTe gamma camera for radioguided surgery and other imaging applications*, *Eur. J. Nucl. Med. Mol. I.* **30** (2003) 1605.

[6] A. Abe, N. Takahashi, J. Lee, T. Oka, K. Shizukuishi, T. Kikuchi, T. Inoue, M. Jimbo, H. Ryuo, and C. Bickel, *Performance evaluation of a hand-held, semiconductor (CdZnTe)-based gamma camera*, *Eur. J. Nucl. Med. Mol. I.* **30** (2003) 805.

[7] A. Ferretti, S. Chondrogiannis, A. Marcolongo and D. Rubello, *Phantom study of a new hand-held gamma-imaging probe for radio-guided surgery*, *Nucl. Med. Commun.* **34** (2013) 86.

[8] W. Xi et al., *MONICA: a compact, portable dual gamma camera system for mouse whole-body imaging*, *Nucl. Med. Biol.* **37** (2010) 245.

[9] C. Trotta, R. Massari, N. Palermo, F. Scopinaro and A. Soluri, *New high spatial resolution portable camera in medical imaging*, *Nucl. Instrum. Meth.*, **A 577** (2007) 604.

[10] P. Olcott, G. Pratx, D. Johnson, E. Mittra, R. Niederkohr and C.S. Levin, *Clinical evaluation of a novel intraoperative handheld gamma camera for sentinel lymph node biopsy*, *Phys. Med.* **30** (2014) 340.

[11] W. Siman and S.C. Kappadath, *Performance characteristics of a new pixelated portable gamma camera*, *Med. Phys.* **39** (2012) 3435.

[12] S. Pitre, L. Menard, M. Ricard, M. Solal, J.R. Garbay and Y. Charon, *A hand-held imaging probe for radio-guided surgery: physical performance and preliminary clinical experience*, *Eur. J. Nucl. Med. Mol. I.* **30** (2003) 339.

[13] I.F. Castro, A.J. Soares, L.M. Moutinho, M.A. Ferreira, R. Ferreira, A. Combo et al., *Characterization of a small CsI(Na)-WSF-SiPM gamma camera prototype using* ^{99m}Tc, 2013 *JINST* **8** C03008.

[14] G.A. de Vree, A.H. Westra, I. Moody, F. van der Have, K.M. Ligtvoet and F.J. Beekman, *Photon-counting gamma camera based on an electron-multiplying CCD*, *IEEE Trans. Nucl. Sci.* **52** (2005) 580.

[15] V.V. Nagarkar, I. Shestakova, V. Gaysinskiy, B. Singh, B.W. Miller and H. Bradford Barber, *Fast X-ray/γ-ray imaging using electron multiplying CCD-based detector*, *Nucl. Instrum. Meth.* **A 563** (2006) 45.

[16] W. Zhao, G. Ristic and J. Rowlands, *X-ray imaging performance of structured cesium iodide scintillators*, *Med. Phys.* **31** (2004) 2594.

[17] S.L. Bugby, J.E. Lees, B.S. Bhatia and A.C. Perkins, *Characterisation of a high resolution small field of view portable gamma camera*, *Phys. Med.* **30** (2014) 331.

[18] B.S. Bhatia, S.L. Bugby, J.E. Lees and A.C. Perkins, *A scheme for assessing the performance characteristics of small field-of-view gamma cameras*, *Phys. Med.* **31** (2015) 98.

[19] *CCD97-00 — Back illuminated 2-phase IMO series peltier pack electron multiplying CCD sensor*, e2v technologies limited, Waterhouse Lane, Chelmsford, Essex, CM1 2QU, England (2011).

[20] *X-Ray Scintillator Technical Information*, Hammamatsu Photonics, Electron Tube Division, 314-5, Shimokanzo, Iwata City, Shizuoka Pref. 438-0193, Japan (2010).

[21] *GOS pixellated scintillator*, Toshiba Materials Co. Ltd., Toshiba Corporation, Yokohama works, 8, Shinsugita-cho, Isogo-ku, Yokohama City.

[22] *NaI(Tl) and Polyscin NaI(Tl) Sodium Iodide Scintillation Material*, Saint-Gobain Crystals, 17900 Great Lakes Parkway, Hiram, OH 44234 (2005).

[23] M.J. Berger et al., *XCOM: photon cross sections database*, *NIST Standard reference database* **8** (1998) 87-3597.

[24] *Scintillation Material Data Sheet — Product: CsI(Tl), CsI(Na), Undoped CsI*, Amcrys, 60, Lenin Ave, Kharkov, 61001 Ukraine (2009).

[25] C.W. Van Eijk, *Inorganic scintillators in medical imaging*, *Phys. Med. Biol.* **47** (2002) R85.

[26] G. Ayotte, L. Archambault, L. Gingras, F. Lacroix, A.S. Beddar and L. Beaulieu, *Surface preparation and coupling in plastic scintillator dosimetry*, *Med. Phys.* **33** (2006) 3519.

[27] D.J. Hall, A. Holland and D.R. Smith, *The use of automatic scale selection to improve the spatial and spectral resolution of a scintillator-coupled EMCCD*, *Nucl. Instrum. Meth.* **A 604** (2009) 207.

[28] S.R. Cherry, J.A. Sorenson and M.E. Phelps, *Physics in Nuclear Medicine*, Elsevier, PA, U.S.A. (2003).

[29] J.H. Hubbell and S.M. Seltzer, *Tables of X-ray mass attenuation coefficients and mass energy-absorption coefficients*, National Institute of Standards and Technology (1996).

[30] S.L. Bugby, J.E. Lees, A.H. Ng, M.S. Alqahtani and A.C. Perkins, *Investigation of an SFOV hybrid gamma camera for thyroid imaging*, *Phys. Med.* **32** (2016) 290.